Journal of Optoelectronic and Biomedical Materials Vol. 16, No. 3, July - September 2024, p. 125 - 139

Theoretical exploration of novel alkannin derived D-π-A conjugated organic dyes as efficient sensitizer in dye-sensitized solar cells

X. Mary Josephine[a*], R. Raj Muhamed[a], V. Sathyanarayanamoorthi[b]
[a] *Department of Physics, Jamal Mohamed College (Autonomous) (Affiliated to Bharathidasan University), Tiruchirappalli-620020, Tamil Nadu, India*
[b]*Department of Physics, PSG College of Arts and Science (Autonomous), Coimbatore-641014, Tamil Nadu, India*

The advancement of cost-effective, highly efficient sensitizers plays a crucial role in the progress of dye-sensitized solar cells (DSSCs). Employing density functional theory (DFT) and time-dependent density functional theory (TD-DFT), a range of metal-free organic dyes with D - π - A configuration, featuring different donor and acceptor groups, have been investigated to enhance the effectiveness of sensitizer dyes. We developed metal-free organic dyes (Ak1-Ak6) with a D - π - A structure through structural modifications of alkannin reference dye. Calculations were conducted to assess the electronic and optical properties, along with key parameters such as short-circuit current density (J_{sc}) and open-circuit voltage (V_{oc}), including light-harvesting efficiency (LHE), electronic injection-free energy (ΔG^{inject}), and regeneration driving forces (ΔG^{reg}) of the designed dyes. The outcomes of this study offer valuable insights for the design of high-efficiency DSSCs.

(Received March 21, 2024; Accepted July 3, 2024)

Keywords: DFT, DSSC, LHE, FMO, Absorption spectra

1. Introduction

Considering urgent environmental concerns such as global warming, fossil fuel depletion, and escalating energy demand, there is a critical need to develop renewable energy technologies that are environmentally friendly [18]. The dye-sensitized solar cell (DSSC), introduced by Gratzel and colleagues [1], represents a novel solar cell type with efficient light-to-electricity conversion capabilities [2]. Positioned as a viable alternative to p-n junction photovoltaic devices [3], the DSSC has garnered considerable attention owing to its flexibility [4], cost-effectiveness [5], environmental friendliness [6], and straightforward fabrication process [7]. The standard DSSC setup includes components arranged in a series, comprising a transparent conducting layer, transparent conducting glass substrate, TiO_2 nanoparticles, dyes, electrolyte, and a counter electrode [8-9]. The operational mechanism of the DSSC involves exciting electrons from the ground state to higher-energy states of the sensitizer, initiated by photon absorption and followed by the injection of the excited electron into the semiconductor conduction band (CB) [10]. The injected electrons are transported by TiO_2 to the conductive contact [12], while the electrolyte reduces oxidized dyes and transports holes to the counter electrode [13-14]. Initially, ruthenium-based complexes gained prominence as photosensitizers due to their favourable photoelectrochemical properties and high stability in the oxidized state [15]. However, their non-biodegradability and carcinogenic nature have led to complex synthesis and design processes, posing substantial environmental and health risks [16-17]. In contrast, the substitution of organic dyes with natural ones that are eco-friendly, biodegradable, and cost-effective opens new avenues for technology commercialization [18]. Metal-free sensitizers, based on the D-π-A architecture, hold promise for high-efficiency photovoltaic output [19]. To explore this potential, we systematically investigated the impact of donor, acceptor, and π-spacer groups on the variable photophysical properties of six newly designed metal-free organic dyes (Ak1-Ak6) for DSSCs,

* Corresponding author: xmaryjosephinemalu@gmail.com
https://doi.org/10.15251/JOBM.2024.163.125

utilizing the D-π-A molecular architecture depicted in Fig. 1. Triphenylamine (TPA) and diphenylamine (DPA) moieties were integrated as electron donors (D), with CN and NO_2 serving as electron acceptors (A), and Alkannin as a π-conjugated system in the D-π-A system as listed in Table1. To assess the influence of auxiliary donors (AD) on photophysical properties, CH_3 groups were incorporated into the TPA donor moiety, as illustrated in Fig. 2. Alkannin, derived from the alkanet root, have high thermal and chemical stability, environmental friendliness, and low production costs, making it a compelling natural-derived dye sensitizer for DSSC applications [20]. The naturally occurring alkannin pigments, chemically iso-hexenylnaphthazarines (5,8-dihydroxy-2-(1-hydroxy-4-methyl-3-pentenyl)-1,4-naphthoquinone), are lipophilic purplish-red pigments [21]. The hydroxyl and carboxylic groups in the alkannin molecule facilitate effective attachment to the surface of the TiO_2 film [22].

2. Computational method

Density functional theory (DFT) calculations were carried out to optimize the ground state geometries of the sensitizers and evaluate electron delocalization in their HOMO-LUMO energy levels [25]. All our theoretical calculations performed by using DFT/B3LYP at the 6–311++*G* (d, p) basis set utilizing the Gaussian 09 software [23]. The Gauss view [24] is employed for the graphical visualizations of the molecule. Frontier molecular orbital (FMO) of the designed dyes were studied to elucidate information about the intermolecular charge transfer within the molecular system using DFT method. Time-dependent density functional theory (TD-DFT) calculations were employed with the same level of theory [26] to investigate the maximum absorption wavelength, vertical excitation energies, oscillator strength of the dyes in both gas and solvent phases. To investigate the solvent effect and predict the optoelectronic properties of the sensitizers, all calculations in the solvent phase used the polarizable continuum model (PCM) of the SCRF method [26]. The solvents used are dimethylformamide (DMF) and dichloromethane (DCM).

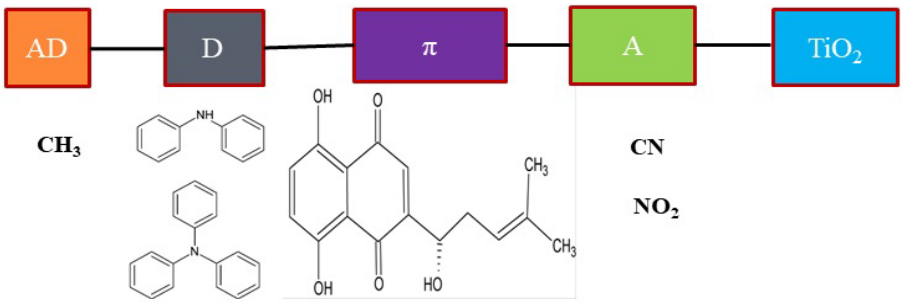

Fig. 1. Molecular architecture of D-π-A system.

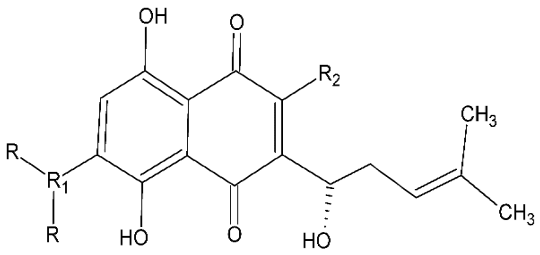

Fig. 2. Chemical structure of newly designed dyes.

Table 1. Donor, acceptor, auxiliary donor for newly designed dyes.

Ak1	R_1= $C_{12}H_{10}N$	R_2= CN	
Ak2	R_1= $C_{18}H_{14}N$	R_2= NO_2	
Ak3	R_1= $C_{12}H_{10}N$	R_2= CN	
Ak4	R_1= $C_{18}H_{14}N$	R_2= NO_2	
Ak5	R_1= $C_{18}H_{14}N$	R_2= CN	R=CH_3
Ak6	R_1= $C_{18}H_{14}N$	R_2= NO_2	R=CH_3

3. Results and discussion

3.1. Geometry optimization

The geometrical characteristics of the proposed sensitizers were determined through density functional theory (DFT) calculations at the B3LYP/6-311++G (d, p) level. Figure 3 illustrates the optimized geometry structures of the dyes. The values of the dihedral angles presented in Table 2. In both gas and solvent phases, the bond lengths (d_1) between the electron-donor moiety and the π-spacer range from 1.419 Å to 1.462 Å. Similarly, the bond length (d_2) between the electron acceptor and the conjugated π-spacer is approximately 1.496 Å in the gas phase and the solvent phases. The relatively shorter bond distances (d_1 and d_2) enhance intramolecular charge transfer (ICT) within the D-π-A molecules [40]. The dihedral angle (ϕ_1) between the donor and the π-spacer remains consistent across all dyes, indicating a planar configuration in the region between the donor and the π-spacer unit. Additionally, the calculated dihedral angles (ϕ_2) between the π-spacer and the acceptor for the designed dyes range from 109.4° to 121.2° in both gas and solvent phases. This variation is attributed to steric repulsion between hydrogen atoms, preventing undesired aggregation of the dye on the semiconductor surface [40]. Despite these variations, no significant differences in bond length were observed across the optimized phases, suggesting that the studied compound possesses favourable properties for designing dye-sensitized solar cells (DSSC).

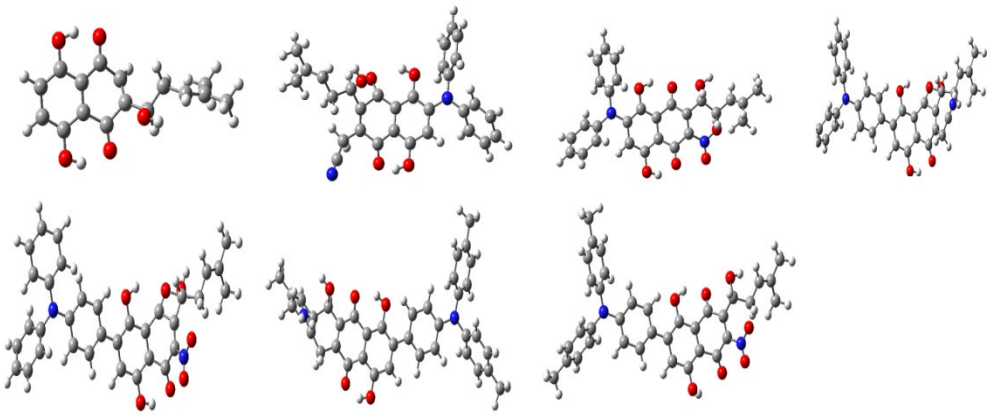

Fig. 3. Optimized geometrical Structure of the designed dyes.

3.2. Frontier molecular orbital (FMO) analysis

The energy of the highest occupied molecular orbital considers as a measure of the ability to donate an electron (HOMO). The lowest unoccupied molecular orbital (LUMO) energy is demonstrated the ability to accept an electron [27]. The gap among the HOMO-LUMO is recognized as band gap energy (E_g) [25]. FMO analysis were carried out at the B3LYP/6-311++G (d, p) level of the theory to calculate the Highest Occupied Molecular Orbital (HOMO) energy is indicative of the electron-donating capability, while the Lowest Unoccupied Molecular Orbital (LUMO) energy signifies the electron-accepting ability [27]. The gap between HOMO and LUMO, recognized as the band gap energy (E_g) [25], was determined through Frontier Molecular Orbital (FMO) analysis at the B3LYP/6-311++G (d, p) level of theory for Ak and Ak1 to Ak6,

with results detailed in Table 3. All designed sensitizers exhibited HOMO energy levels below the redox potential of iodine/tri-iodide (I^-/I^{3-}), except Ak5, suggesting the potential for electrolyte electrons to reduce oxidized molecules. Additionally, the designed sensitizers possessed LUMO values higher than the conduction band (CB) of TiO_2 (−4.00 eV) [36], indicating swift electron injection into the TiO_2 conduction band during sensitization. The energy levels of HOMO, LUMO, and the band gap (E_g) are graphically depicted in Fig. 5, revealing that Ak1, Ak2, Ak3, Ak4, and Ak6 exhibited superior regeneration capacities compared to Ak5. Table 3 provides details on the HOMO-LUMO and energy gap of the designed dyes in various solvent media. A smaller bandgap energy in a sensitizer is advantageous for enhanced electron excitation and absorption properties, potentially increasing short-circuit current density (J_{sc}) [28]. Table 3 indicates that the largest (E_g) value is 3.1268 in the reference dye (Ak). Designed sensitizers Ak1 to Ak6 exhibited smaller (E_g) values than Ak, suggesting their potential for superior J_{sc}. The incorporation of donor and acceptor units in the π-conjugated system resulted in a reduced band gap in the designed photosensitizers. Ak5 displayed the smallest HOMO-LUMO energy gap at 1.2394 eV, followed by Ak6 (1.8057 eV) due to the coupling of the auxiliary donor group. Structural tailoring of the reference dye (Ak) significantly reduced the energy gap across all designed sensitizers. Consequently, Ak1 to Ak6 are deemed effective photosensitizers suitable for Dye-Sensitized Solar Cell (DSSC) applications. Analysis of HOMO and LUMO distributions pattern depicted in figure (4) revealed that in Ak dye, these orbitals spread across the entire molecule. For Ak1, Ak2, Ak3, Ak4 and Ak5, HOMO electrons were widely distributed, with maximum density on the π spacer system. LUMOs were situated extensively over acceptor units and partially on the π-conjugated system. In Ak6, HOMOs were heavily localized on the π-conjugated system and partially on the donor unit, while LUMOs were partially populated on the π-conjugated system and the acceptor region. The auxiliary donor group had no significant contribution to HOMO. There is an efficient charge transfer from the donor unit to the acceptor unit through the π-conjugated spacer in all designed sensitizers. The improved Intramolecular Charge Transfer (ICT) behaviour further indicates that Ak1 to Ak6 are excellent materials for photosensitization.

Table 2. Optimized bond lengths and dihedral angles of the dyes at the at B3LYP/ 6-311++G (d, p) level of theory.

Dye	GAS PHASE				DMF				DCM			
	d_1	**d_2**	**ϕ_1**	**ϕ_2**	**d_1**	**d_2**	**ϕ_1**	**ϕ_2**	**d_1**	**d_2**	**ϕ_1**	**ϕ_2**
Ak1	1.462	1.497	120.0	109.4	1.462	1.497	120.0	109.4	1.462	1.497	120.0	109.4
Ak2	1.462	1.496	120.0	121.2	1.462	1.496	120.0	121.2	1.462	1.496	120.0	120.2
Ak3	1.402	1.497	120.0	110.2	1.420	1.497	120.0	110.2	1.420	1.497	120.0	110.2
Ak4	1.420	1.496	120.0	120.0	1.420	1.496	120.0	120.0	1.420	1.496	120.0	120.0
Ak5	1.420	1.497	120.0	109.4	1.420	1.497	120.0	120.5	1.420	1.497	120.0	120.5
Ak6	1.419	1.496	120.6	120.0	1.419	1.496	120.6	120.0	1.419	1.496	120.6	120.0

Table 3. Calculated E_{HOMO}, E_{LUMO} and energy gap (E_g) of Alkannin and designed dyes in eV at B3LYP/6-311++G (d, p) level of theory.

Dye	GASPHASE			DMF			DCM		
	HOMO	**LUMO**	**E_{gap}**	**HOMO**	**LUMO**	**E_{gap}**	**HOMO**	**LUMO**	**E_{gap}**
Ak	-6.4037	-3.2768	3.1268	-6.4004	-3.2762	3.1241	-6.3813	-3.2724	3.1089
Ak1	-5.8934	-3.0765	2.8169	-5.9019	-3.1105	2.7913	-5.9019	-3.1105	2.7913
Ak2	-4.3280	-2.2871	2.0408	-4.5726	-2.6572	1.9154	-4.5394	-2.6049	1.9344
Ak3	-5.4991	-2.9935	2.5056	-5.5392	-3.0055	2.5304	-5.5225	-3.0047	2.5178
Ak4	-5.6496	-3.7198	1.9298	-5.6025	-3.7519	1.8506	-5.5996	-3.7508	1.8487
Ak5	-4.2267	-2.9872	1.2394	-4.0874	-3.0947	0.9926	-4.1073	-3.088	1.0264
Ak6	-5.4532	-3.6474	1.8057	-5.5092	3.7227	1.7869	-5.4929	-3.7200	1.7772

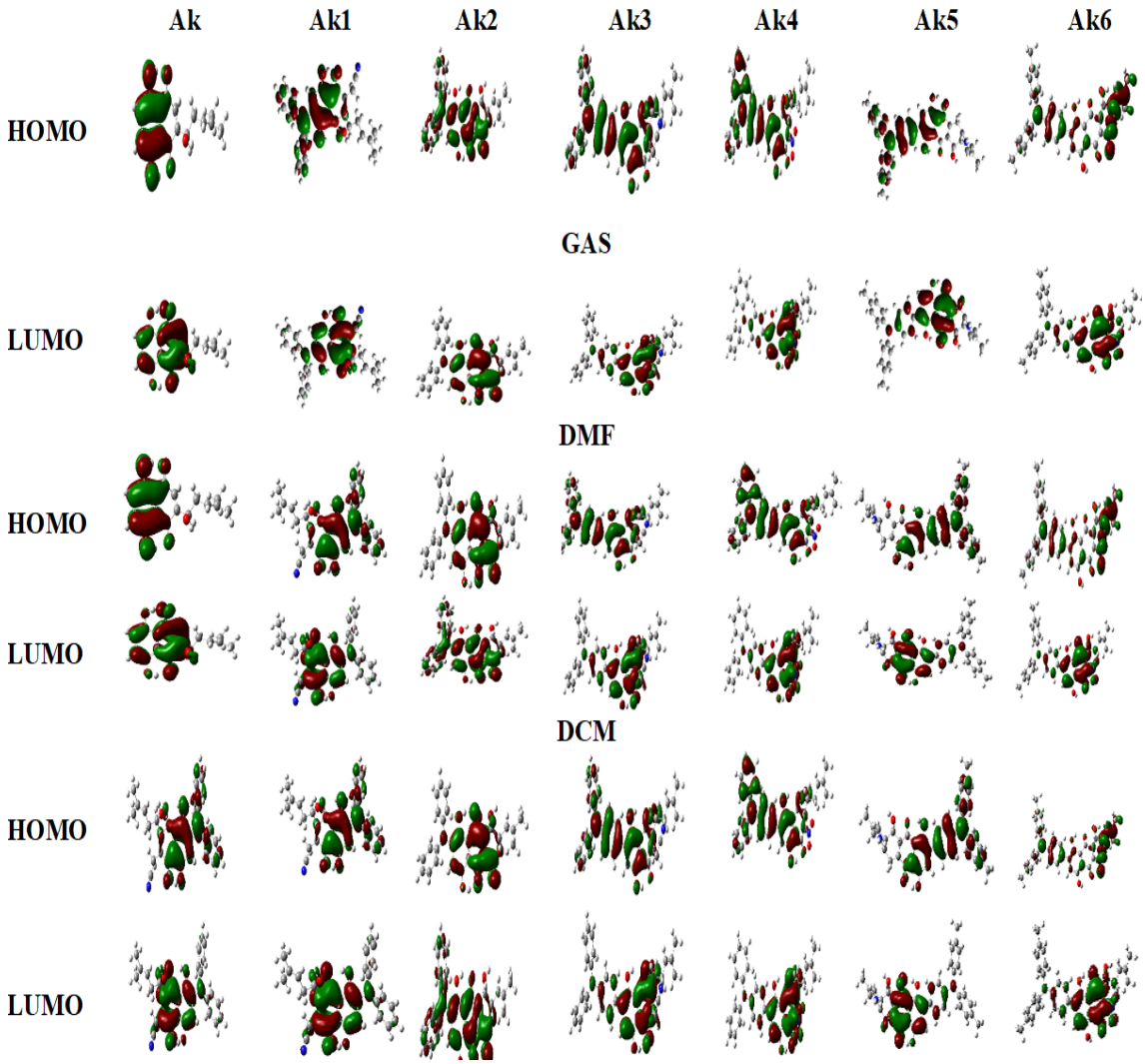

Fig. 4. HOMO and LUMO orbitals of Alkannin and designed dyes in gas phase.

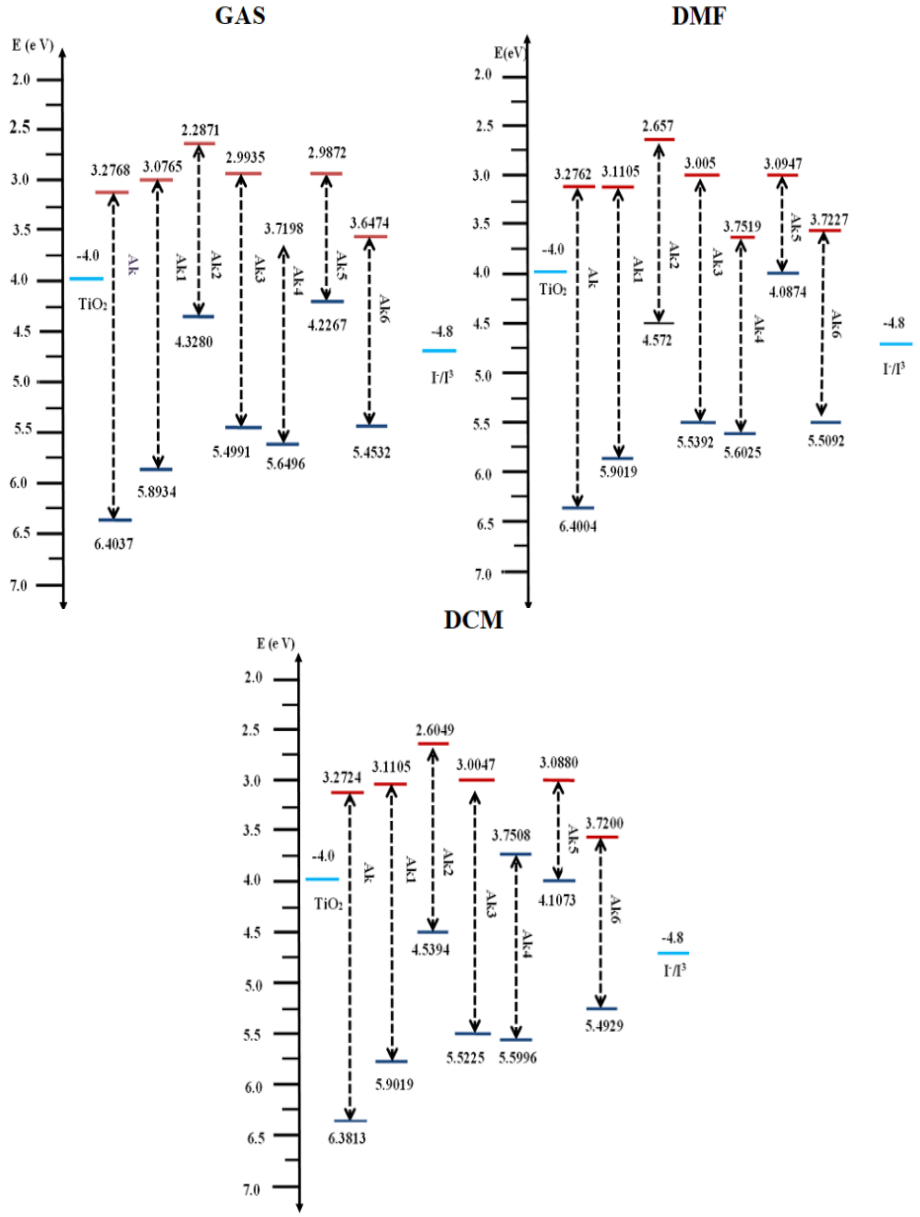

Fig. 5. HOMO, LUMO energies and energy gap of alkannin and designed dyes in Gas phase, DMF and DCM solvent phase.

3.3. Photovoltaic properties

The efficiency of DSSCs can be estimated by considering photovoltaic properties. These include light harvesting efficiency (LHE), ground state oxidation potential (E_{ox}^{dye}), excited state oxidation potential ($E_{ox}^{dye^*}$), negative free energy of injection (ΔG^{inject}), electron regeneration energy (ΔG^{reg}), open-circuit voltage (V_{OC}), and electron coupling constant (V_{RP}) of the dye.

3.3.1. Light harvesting efficiency (LHE)

Light harvesting efficiency (LHE) is the fraction of light intensity absorbed by the dye molecules [25]. The LHE must be high to enhance the photocurrent reaction. The higher the oscillator strength, the more LHE, as described in Eq. (1) [30].

$$LHE = 1 - 10^{-f} \quad (1)$$

where f is the oscillator strength at the maximum absorption peak obtained from the TDDFT calculations, directly [30]. According to the Table 4, Solvents enhance the LHE of the dyes through the increase in the oscillator strength, i.e., the solvents may increase the probability of the electronic transitions between the corresponding energy levels, and therefore increase the oscillator strength (f), which is related to the strength of the electronic transitions [31]. The values of LHE increase in the following order; Ak3 > Ak4 > Ak5 > Ak6 > Ak2 > Ak1> Ak for gas and solvent phases respectively. Lowest LHE value is measured in the reference dye Ak. Structural modification also increases the LHE values in Ak1 to Ak6. Among the investigated dyes Ak3 and Ak4 had the highest values of light harvesting efficiencies due to strong electron donating capability. Hence these dyes are suggested to be a suitable candidate in the DSSCs application.

3.3.2. Electron injection efficiency (ΔG^{inject})

The process of electron injection from the excited dye to the semiconductor's conduction band (CB) and subsequent dye regeneration are described as charge transfer (CT) reactions [31]. According to Marcus theory, the free energy change in the electron transfer reaction influences the CT rate constants [32]. The efficiency of dye molecules in injecting electrons from the lower unoccupied molecular orbital (LUMO) to the semiconductor's conduction band is termed electron injection efficiency [31]. This efficiency is determined by Eq. (2) [33]:

$$\Delta G^{\text{inject}} = E_{ox}^{dye^*} - E_{CB}^{TiO_2} \quad (2)$$

where $E_{ox}^{dye^*}$ is the oxidation potential energy in excited state [33], $E_{CB}^{TiO_2}$ is the reduction potential of the semiconductor whose value is -4.0eV [36]. The oxidation potential energy of the dye in an excited state can be calculated by Eq. (3)[33].

$$E_{ox}^{dye^*} = E_{ox}^{dye} - \lambda_{max}^{ICT} \quad (3)$$

where, E_{ox}^{dye} is the dye's oxidation potential energy in the ground state, λ_{max}^{ICT} is the vertical electronic transition energy corresponding to the wavelength maximum (λ^{max}) [34].The negative ΔG^{inject}values demonstrated that for all designed dyes Ak1-Ak6 the excited states of the dyes lie above the conduction band edge of TiO_2 and electron injection from the dye to a semiconductor conduction band is a spontaneous process [33]. The ΔG^{inject} values acquired in both gas and solvent phases suggest that the stability of electron injection and oxidation potential can be influenced by the electrostatic interaction of the medium [31].

3.3.3. Electron regeneration energy (ΔG^{reg})

The electron regeneration efficiency of a dye, which is its ability to regain electrons from the electrolyte after being photoexcited, is a key factor that affects the performance of dye-sensitized solar cells (DSSCs) [35-36]. It is calculated using equation (4), and the results are shown in Table 5.

$$\Delta G^{reg} = E_{ox}^{dye} - E^{-}_{I}/I_3^- \quad (4)$$

where E^{-}_{I}/I_3^-Is the redox potential of electrolyte which is given as (-4.85 eV) [36]. To get fast electron transfer, ΔG^{reg} must be as low as possible [37]; Table 5 shows that all the studied dyes Ak1-Ak6 can efficiently regenerate electrons from the electrolyte, as indicated by their lower ΔG^{reg} values than the reference molecule Ak, which suggests that they have a greater power conversion efficiency.

3.3.4. Open circuit voltage (V_{OC})

Power conversion efficiency (η) in dye-sensitized solar cells (DSSCs) can be estimated using the open-circuit voltage (V_{OC}) [34]. Electron transfer occurs from the lowest unoccupied molecular orbital (LUMO) of the dye molecules to the conduction band of the semiconductor, so a

higher LUMO energy level leads to a higher (V_{OC}) [31]. The (V_{OC}) is calculated using the following equation:

$$V_{OC} = E_{LUMO} - E_{CB} \quad (5)$$

As depicted in Table 6 the designed dyes Ak1, Ak2, Ak3 and Ak5 exhibited higher value of (V_{OC}) compared with the reference dye Ak. Due to lowering of LUMO values Ak4 and Ak6 show least value of V_{OC}.

Table 4. Absorption peak maxima (λ_{max}), Oscillator Strength (f), Light Harvesting Efficiency (LHE), average Light Harvesting Efficiency (LHE_{avg}), of Alkannin and designed dyes.

DYE	GAS PHASE				DMF				DCM			
	λ_{max}	**f**	**LHE**	**LHE_{avg}**	**λ_{max}**	**f**	**LHE**	**LHE_{avg}**	**λ_{max}**	**f**	**LHE**	**LHE_{avg}**
Ak	486.16 478.41	0.0063 0.0881	0.0144 0.1836	0.0990	486.22 479.90	0.0102 0.0882	0.0232 0.1837	0.1034	485.85 481.29	0.0455 0.0508	0.0994 0.1103	0.1048
Ak1	526.59 424.52	0.1504 0.0333	0.2927 0.0738	0.1832	537.44 427.29	0.1953 0.0462	0.3621 0.0884	0.2252	537.44 427.29	0.1953 0.0402	0.3621 0.0884	0.2252
Ak2	855.46 467.68	0.0135 0.1844	0.0306 0.3459	0.1882	829.46 440.76	0.0849 0.2822	0.1775 0.4778	0.3276	818.50 439.65	0.0861 0.2620	0.1798 0.4529	0.3163
Ak3	568.79 427.97	0.3343 0.1500	0.5368 0.2920	0.4144	570.77 365.97	0.4585 0.4761	0.6520 0.6658	0.6589	573.96 366.85	0.4488 0.4653	0.6442 0.6574	0.6508
Ak4	776.28 474.73	0.0800 0.4599	0.1682 0.6531	0.4106	824.21 509.46	0.0727 0.5197	0.1541 0.6977	0.4259	824.55 507.24	0.0770 0.4936	0.1624 0.6790	0.4207
Ak5	733.05 619.09	0.0292 0.3035	0.0650 0.5028	0.2839	850.12 623.03	0.0274 0.3794	0.0611 0.5825	0.3218	832.77 627.83	0.0282 0.3803	0.0628 0.5834	0.3231
Ak6	846.52 501.48	0.0944 0.1197	0.1953 0.2408	0.2180	862.81 485.77	0.1167 0.2190	0.2356 0.3960	0.3158	871.07 486.76	0.1181 0.2209	0.2380 0.3986	0.3183

Table 5. Calculated maximum absorption wavelength (λ_{max}), vertical excitation energy, excited state oxidation potential, Electron injection efficiency (ΔG^{inject}), Electron regeneration energy (ΔG^{reg}) of Alkannin and designed dyes.

DYE	GAS PHASE					DMF					DCM				
	λ_{max}	λ_{max}^{ICT}	E_{ox}^{dye*}	ΔG^{inject}	ΔG^{reg}	λ_{max}	λ_{max}^{ICT}	E_{ox}^{dye*}	ΔG^{inject}	ΔG^{reg}	λ_{max}	λ_{max}^{ICT}	E_{ox}^{dye*}	ΔG^{inject}	ΔG^{reg}
Ak	486.16	2.5503	3.8534	-0.1466	1.5537	486.22	2.5499	3.8505	-0.1495	1.5504	485.85	2.5519	3.8234	-0.1766	1.5313
Ak1	526.59	2.3545	3.5389	-0.4611	1.0434	537.44	2.3069	3.8505	-0.1495	1.0519	537.44	2.3069	3.5950	-0.4050	1.0519
Ak2	855.46	1.4493	2.8787	-1.1213	-0.5220	829.46	1.4948	3.0778	-0.9222	-0.2774	818.50	1.5148	3.0246	-0.9754	-0.3106
Ak3	568.79	2.1798	3.3193	-0.6807	1.0065	570.77	2.1722	3.3670	-0.6330	0.6892	573.96	2.1602	3.3623	-0.6377	0.6725
Ak4	776.28	1.6972	4.1252	-0.0476	0.7996	824.21	1.6043	3.9595	-0.0405	0.7525	824.55	1.7035	1.8487	-0.1041	0.7496
Ak5	733.05	1.6914	2.5353	-1.4647	-0.6233	626.97	1.9775	2.1099	-1.8901	-0.7626	832.77	1.4888	2.6185	-1.3815	-0.7427
Ak6	846.52	1.4646	3.9886	-0.0114	0.6032	862.81	1.5370	3.9722	-0.0278	0.6592	871.07	1.5234	3.9695	-0.0305	0.6429

Table 6. The open-circuit Voltage (V_{OC}) and electron coupling constants ($|V_{RP}|$) in eV.

DYE	GAS PHASE		DMF		DCM	
	V_{oc}	**V_{RP}**	**V_{oc}**	**V_{RP}**	**V_{oc}**	**V_{RP}**
Ak	0.7232	1.2018	0.7238	1.2002	0.7276	1.1906
Ak1	0.9235	0.9467	0.8895	0.9509	0.8895	0.9509
Ak2	1.7129	0.1640	1.3428	0.2863	1.3951	0.2697
Ak3	1.0065	0.7495	0.9950	0.7696	0.9953	0.7612
Ak4	0.2802	0.8248	0.2481	0.8012	0.2492	0.7998
Ak5	1.0128	0.1133	0.9053	0.0437	0.9192	0.0536
Ak6	0.3526	0.7266	0.2773	0.7546	0.2800	0.7464

3.3.5. Electronic coupling constant (V_{RP})

From Generalized Milliken – Hush (GMH) formalism the coupling constant can be evaluated from Eqs. (6) and (7) as follows [38].

$$V_{RP} = \frac{\Delta E_{RP}}{2} \tag{6}$$

The injection driving force can be expressed within Koopmans approximation as [39]

$$\Delta E_{RP} = [E_{LUMO}^{dye} + 2E_{HOMO}^{dye}] - [E_{LUMO}^{dye} + E_{HOMO}^{dye} + E_{CB}^{TiO2}] \tag{7}$$

Thus equation (7) could be represented as

$$\Delta E_{RP} = [E_{HOMO}^{dye} + E_{CB}^{TiO2}] = -[E_{OX}^{dye} + E_{CB}^{TiO2}] \tag{8}$$

The electron coupling constant between two states is a measure of the strength of the interaction between them. As depicted in Table 6 a higher electron coupling constant of the designed dyes Ak1 to Ak6 indicates that the electrons can move between the two states more easily.

3.3.6. UV–Vis spectra of studied compounds

UV–Vis spectroscopy offers thoughtful insight about the electronic transition nature, and probability of charge transfer within the molecules [25]. The excited state absorption spectra of Ak and Ak1-Ak6 were stimulated using TD-DFT computations at B3LYP/6-311++G (d, p) level of theory in conjunction with PCM model using DMF and DCM as solvent. absorption spectra of Ak and Ak1-Ak6 are depicted in Fig. 6. For all the designed dyes, the absorption spectrum has red shifted widely, with an increase in the absorption peak. Therefore, structural modifications of reference dye (Ak) red shifted the absorption spectrum of designed dyes (Ak1-Ak6) respectively.

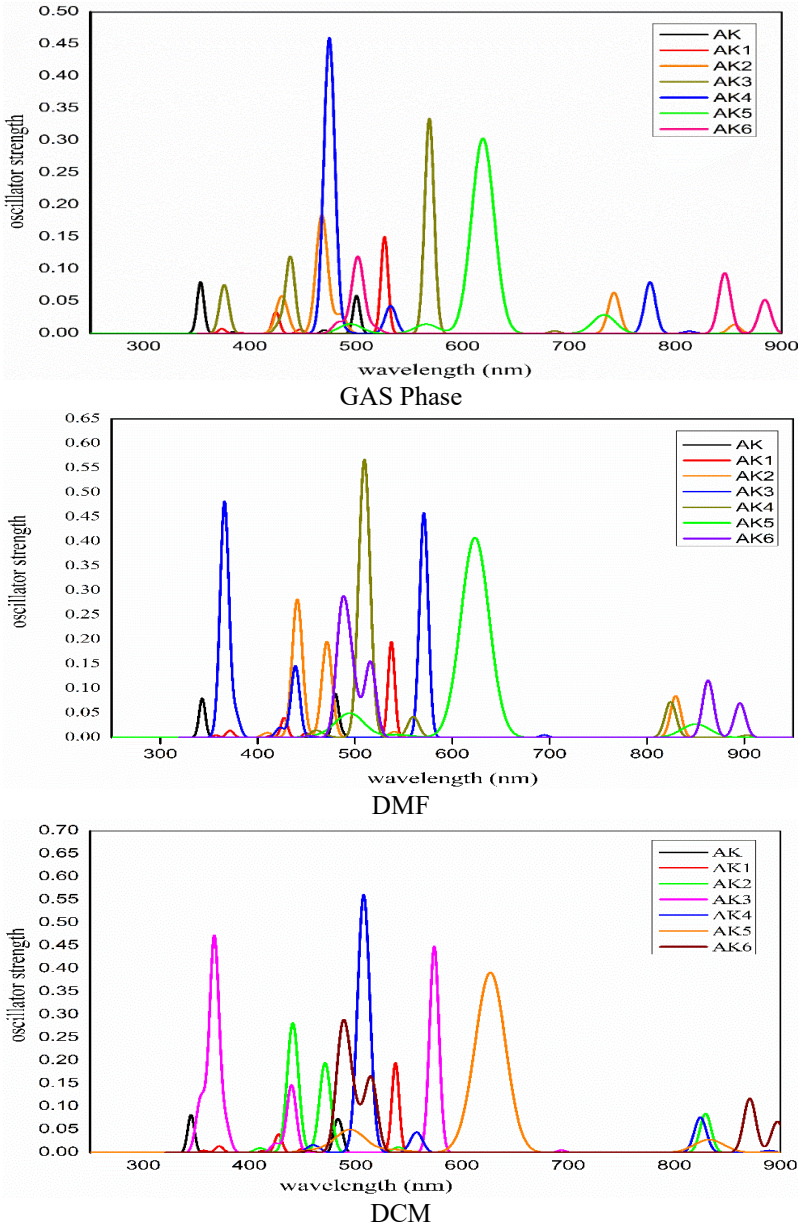

Fig. 6. Stimulated UV-visible absorption spectra of Alkannin and designed dyes in (a) gas phase (b) DMF (c) DCM.

3.4. Molecular electrostatic potential (MEP) surface

The molecular electrostatic potential (MEP) surface of the designed dyes was calculated using DFT/B3LYP with a 6-311++G (d, p) basis set, and the resulting MEP surface is illustrated in Fig. 7.

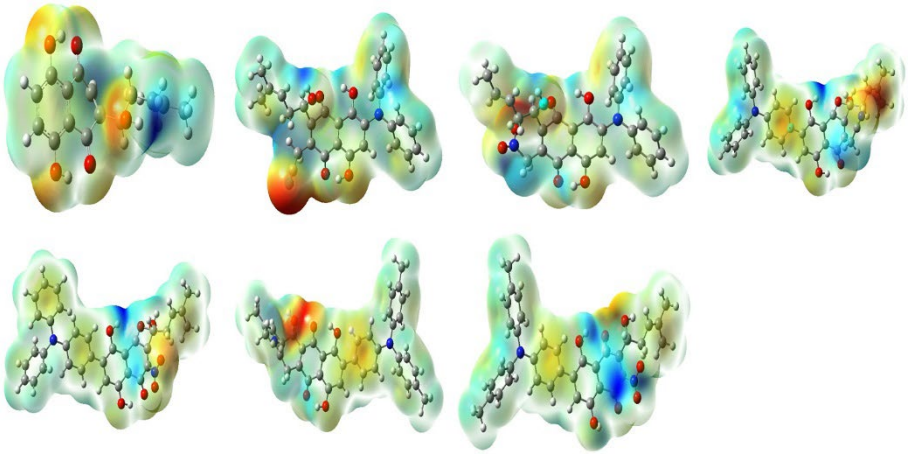

Fig. 7. Molecular electrostatic potential diagram of the designed dye.

MEP is a valuable tool for identifying sites prone to electrophilic attacks, nucleophilic reactions, and hydrogen-bonding interactions [41]. The electrostatic potential is depicted through colors, where increasing potential is represented by red > orange > yellow > green > blue [42]. Reactive regions are highlighted with red indicating electrophilic reactivity and blue indicating nucleophilic reactivity [41]. Negative electrostatic potentials (depicted in red) around the oxygen in the π spacer and nitrogen atoms of the anchoring acceptor group indicate their negative partial charges. These sites are potentially susceptible to electrophilic attacks from the electrolyte. Additionally, a positive potential site, represented by a blue colour and associated with hydrogen bonded to carbon atoms in the overall ring, is exposed to nucleophilic attack. This information aids in understanding the potential reactivity of specific regions in the molecular structure.

3.5. Global molecular reactivity descriptors

The molecular characteristics, including properties such as Ionization Potential (IP), Electron Affinity (EA), electronegativity (χ), electrophilicity index (ω), hardness (η), softness (S), and chemical potential (μ), were determined using HOMO and LUMO energy values, applying Koopman's theorem [45-46] by utilizing the equations (9) to (14), and are presented in Table 7. The Ionization Potential (IP) and Electron Affinity (EA) are defined as IP = $-E_{HOMO}$ and EA = $-E_{LUMO}$ [43-44].

$$\mu = \frac{IP+EA}{2} \tag{9}$$

$$\eta = \frac{IP-EA}{2} \tag{10}$$

$$S = \frac{1}{\eta} \tag{11}$$

$$\omega = \frac{\mu^2}{2\eta} \tag{12}$$

$$\omega^+ = \frac{(IP+3EA)^2}{16(IP-EA)} \tag{13}$$

$$\omega^- = \frac{(3IP+EA)^2}{16(IP-EA)} \tag{14}$$

Ak5 exhibits the lowest ionization Potential (IP), indicating a greater ease of losing electrons compared to other dyes. Conversely, Ak6 displays the highest Electron Affinity (EA), suggesting a strong inclination to accept electrons. The relationship between hardness (η) and softness (S) is inversely proportional and is crucial in determining charge transfer resistance. Compounds with higher hardness values demonstrate greater chemical stability. Similarly,

chemical potential (μ) reveals the tendency to lose electrons under equilibrium conditions. Table 7 indicates that the η values of the designed dyes are lower than those of the reference dye Ak. Notably, Ak5 exhibits the lowest chemical hardness and highest softness among the studied dyes, suggesting lower resistance to intramolecular charge transfer. The values above imply a reciprocal relationship between hardness and softness. It is observed that the conversion efficiency increases as chemical hardness decreases. Considering electrophilicity, higher electrophilicity contributes to increased energetic stability by acquiring electrons from the environment, leading to improved conversion efficiency. Among the designed dyes, Ak6 possesses the highest electrophilicity value. The tendency to accept or donate charge can be analysed using ω+ and ω− expressed in Equations (4) and (5). For electro-donating power (ω−), low values imply a strong capability to donate electrons, while for electro-accepting power (ω+), high values imply a strong capability to accept electrons. Among the studied dyes, Ak4 and Ak6 exhibit the highest electron-accepting power, and Ak2 demonstrates high electron-donating power. Additionally, the calculated electron-donating powers of the reference and designed dyes (Ak) display the same trend of electrophilicity and electron-accepting power. The study indicates that lower chemical hardness corresponds to higher electron-accepting power, leading to a better short-circuit current density and improved light conversion efficiency for the designed dyes Ak4-Ak6.

Table 7. The ionization potential (IP) electron affinity (EA), chemical potential (μ), chemical hardness (η), softness(S), electrophilicity (ω), electron donating power (ω-), and electron accepting power (ω+) in eV calculated at B3LYP/6-311++ G (d, p) level of theory.

Dye	IP	EA	μ	η	S	ω	ω^+	ω^-
Ak	6.4037	3.2768	4.8402	1.5634	0.6396	7.4924	5.2677	10.1079
Ak1	5.8934	3.0765	4.4849	1.4084	0.7100	7.1407	5.0743	9.5592
Ak2	4.3280	2.2871	3.3075	1.0204	0.9799	5.3603	3.8341	7.1416
Ak3	5.4991	2.9935	4.2463	1.2528	0.7982	7.1963	5.2297	9.4760
Ak4	5.6496	3.7198	4.6847	0.9649	1.0363	11.3723	9.1506	13.8353
Ak5	4.2267	2.9872	3.6069	0.6197	1.6135	10.4962	8.7702	12.3771
Ak6	5.4532	3.6474	4.5503	0.9029	1.1075	11.4659	9.3036	13.8539

4. Conclusion

We designed six new D-π-A dyes (Ak1-Ak6) by structurally modifying the reference dye (Ak). These dyes have significantly enhanced photophysical properties. We used DFT and TD-DFT methods to investigate the geometry, electronics, and optoelectronic characteristics of the reference and designed dyes for DSSC devices. Our calculations suggest that the designed dyes would exhibit better optical and electrical properties than the reference dye. This is due to their smaller energy gaps, red-shifted absorption spectra, larger λ_{max}, higher LHE values, suitable FMO energy levels, and decreasing ΔG^{reg}. Therefore, the designed dyes (Ak1-Ak6) are more promising candidates for use in DSSCs.

References

[1] O'Regan, B., Gratzel, M. Nature, (1991),353, 737-740; https://doi.org/10.1038/353737a0

[2] Gonçalves, L. M., de Zea Bermudez, V., Ribeiro, H. A., Mendes, A. MEnergy & Environmental Science. (2008),1(6), 655; https://doi.org/10.1039/b807236a

[3] Zhang, J., Li, H. B., Sun, S. L., Geng, Y., Wu, Y., Su, Z. M. Journal of Materials Chemistry. (2012), 22(2), 568-576; https://doi.org/10.1039/C1JM13028E

[4] Yang, Z., Liu, C., Li, K., Cole, J. M., Shao, C., Cao, D. ACS Applied Energy Materials. 2018, 1, 1435-1444; https://doi.org/10.1021/acsaem.7b00154

[5] Krishna, N. V., Krishna, J. V., Mrinalini, M., Prasanthkumar, S., Giribabu, L. ChemSusChem. 2017, 23, 4668-4669; https://doi.org/10.1002/cssc.201701224

[6] Ambre, R. B., Mane, S. B., Hung, C. H. Energies. 2016, 9, 513-524; https://doi.org/10.3390/en9070513

[7] Kim, G., Noh, Y., Choi, M., Kim, K., Song, O. Journal of the Korean Ceramic Society. 2016, 53(2), 110-115; https://doi.org/10.4191/kcers.2016.53.1.110

[8] Yen, Y.-S., Chou, H.-H., Chen, Y.-C., Hsu, C.-Y., Lin, J. TJournal of Materials Chemistry. 2012, 22(19), 8734-8747; https://doi.org/10.1039/c2jm30362k

[9] Peng, M., Yan, K., Hu, H., Shen, D., Song, W., Zou, D. (2015). Journal of Materials Chemistry C, 2015, 3, 2157-2165; https://doi.org/10.1039/C4TC02997F

[10] Gebeyehu, D., Brabec, C. J., Sariciftci, N. S., Vangeneugden, D., Kiebooms, R., Vanderzande, D. Synthetic Metals. 2002, 125(2-3), 279-287; https://doi.org/10.1016/S0379-6779(01)00395-2

[11] Liu, S. H., Fu, H., Cheng, Y. M., Wu, K. L., Ho, S. T., Chi, Y. The Journal of Physical Chemistry C. 2012, 116 (31), 16338-16345; https://doi.org/10.1021/jp3006074

[12] Docampo, P., Guldin, S., Leijtens, T., Noel, N. K., Steiner, U., Snaith, H. J. Advanced Materials. 2014. 26(25), 4013-4030; https://doi.org/10.1002/adma.201400486

[13] Wu, J., Lan, Z., Lin, J., Huang, M., Huang, Y., Fan, L. Chemical Reviews. 2015, 115(5), 2136-2173; https://doi.org/10.1021/cr400675m

[14] Yun, S., Lund, P. D., Hinsch, A. Energy & Environmental Science. 2015, 8(12), 3495-3514; https://doi.org/10.1039/C5EE02446C

[15] Kohle, O., Grätzel, M., Meyer, A. F. Advanced Materials. 1997, 9 (11), 904-906; https://doi.org/10.1002/adma.19970091111

[16] Batlle, A. M. C., Journal of Photochemistry and Photobiology B: Biology. 1993, 20 (1), 5-22; https://doi.org/10.1016/1011-1344(93)80127-U

[17] Chung, K. T. Mutation Research/Reviews in Genetic Toxicology. 1983, 114 (3), 269-281; https://doi.org/10.1016/0165-1110(83)90035-0

[18] Narayan, M. R. Renewable and Sustainable Energy Reviews. 2012, 16(1), 208-215.

[19] Chen, Z., Li, F., Huang, C. Current Organic Chemistry. 2007,11 (14), 1241-1258; https://doi.org/10.2174/138527207781696008

[20] Kushwaha, S., & Bahadur, L. In 2012 Students Conference on Engineering and Systems. IEEE. 2012.

[21] Calogero, G., Di Marco, G. Solar Energy. 2008, Journal of Environmental Nanotechnology, 2016, 5(3), 44-50.

[23] Frisch, M. J., Trucks, G. W., et al. (2009). Gaussian 09 W, Revision D.01. Wallingford, CT: Gaussian Inc.

[24] Nielsen, A. B., Holder, A. J. Gauss View 5.0 User's Reference. Pittsburgh: Gaussian Inc.

[25] Roohi, H., Motamedifar, N. Molecular Physics. 2021,119 (10); https://doi.org/10.1080/00268976.2021.1913250

[26] Kanchana, T., Kaviya, P., Rajkumar, M., Dhinesh Kumar, N., Elangovan, S., Sowrirajan, S. Chemical Physics Impact. 2023, 7. 100263.

[27] Manjusha, P., Prasana, J. C., Muthu, S., Raajaraman, B. R. Journal of Molecular Structure. 2020, 1203, 127394; https://doi.org/10.1016/j.molstruc.2019.127394

[28] Mu˜noz-Garc'ıa, A. B., Benesperi, I., Boschloo, G., Concepcion, J. J., Delcamp, J. H., Gibson, E. A., Meyer, G. J., Pavone, M., Pettersson, H., Hagfeldt, A., Freitag, M. Chemical Society Reviews, 2021, 50, 12450-12550; https://doi.org/10.1039/D0CS01336F

[29] Kershaw, S. V., Jing, L., Huang, X., Gao, M., Rogach, A. L. Materials Horizons. 2017, 4, 155-205; https://doi.org/10.1039/C6MH00469E

[30] Fan, W. J., Tan, D. Z., Deng, W. QChemPhysChem, 2012, 13(8), 2051-2060; https://doi.org/10.1002/cphc.201200064

[31] Arkan, F., Izadyar, M., Nakhaeipour, A.. Energy. 2016, 114, 559-567;

https://doi.org/10.1016/j.energy.2016.08.027
[32] Zhang, Z. L., Zou, L. Y., Ren, A. M., Liu, Y. F., Feng, J. K., Sun, C. C. Dyes and Pigments, 2013, 96, 349-363; https://doi.org/10.1016/j.dyepig.2012.08.020
[33] Xie, M., Wang, J., Xia, H.-Q., Bai, F.-Q., Jia, R., Rim, J.-G., Zhang, H.-X. RSC Advances. 2015, 5(42), 33653-33665; https://doi.org/10.1039/C4RA17080F
[34] Kacimi, R., Bourass, M., Toupance, T., Wazzan, N., Chemek, M., El Alamy, A., Bejjit, L., Alimi, K., Bouachrine, M. Research on Chemical Intermediates, 2020, 46, 3247-3262; https://doi.org/10.1007/s11164-020-04150-7
[35] Zhang, C. R., Liu, L., Zhe, J. W., Jin, N. Zh., Ma, Y., Yuan, L. H. International Journal of Molecular Sciences, 2013, 14(3), 5461-5481; https://doi.org/10.3390/ijms14035461
[36] Li, Y., Sun, C., Song, P., Ma, F., Yang, Y. ChemPhysChem. 2017,18(4), 366-383; https://doi.org/10.1002/cphc.201601101
[37] Galappaththi, K., Ekanayake, P., Petra, M. I. Solar Energy. 2018,16, 83-89; https://doi.org/10.1016/j.solener.2017.12.027
[38] Cave, R. J., Newton, M. D. Journal of Chemical Physics. 1997, 106, 9213-9226; https://doi.org/10.1063/1.474023
[39] Hsu, C. P. Accounts of Chemical Research. 2009, 42, 509-518. https://doi.org/10.1021/ar800153f
[40] Biswas, A. K., Das, A., Ganguly, B. New Journal of Chemistry, 40(11), 9304-9312; https://doi.org/10.1039/C6NJ02040B
[41] Zhou, C.-H., Zhao, X. J. Organomet. Chem. 2011, 696, 3322-3327; https://doi.org/10.1016/j.jorganchem.2011.07.003
[42] El Kalai, F., et al. Journal of Molecular Structure. 2021, 1223, 129213; https://doi.org/10.1016/j.molstruc.2020.129213
[43] Delgado, J. C., Ishikawa, Y., Selby Journal of Molecular Structure. 2018, 1160, 271-292; https://doi.org/10.1016/j.molstruc.2018.01.083
[45] Altürk, S., Avcı, D., Tamer, O. Atalay, Y., Sahin, O. Journal of Physical Chemistry Solids. 2016, 98, 71-80; https://doi.org/10.1016/j.jpcs.2016.06.008
[46] Yang, R. G., Parr, Proceedings of the National Academy of Sciences. 1985, 82(19), 6723-6726; https://doi.org/10.1073/pnas.82.20.6723